AIAA-95-1848
Subsonic-to-Hypersonic Aerodynamic Characteristics for a Winged, Circular-Body, Single-Stage-to-Orbit Spacecraft Configuration

W. P. Phillips and W. C. Engelund
NASA Langley Research Center
Hampton, VA

AIAA Applied Aerodynamics Conference
June 19 - 22,1995 / San Diego, CA

SUBSONIC-TO-HYPERSONIC AERODYNAMIC CHARACTERISTICS FOR A WINGED, CIRCULAR-BODY, SINGLE-STAGE-TO-ORBIT SPACECRAFT CONFIGURATION

W. Pelham Phillips* and Walter C. Engelund§
NASA-Langley Research Center
Hampton, Virginia 23681-0001

ABSTRACT

Experimental aerodynamic characteristics were obtained for a generic, winged, circular-body, single-stage-to-orbit spacecraft configuration. The baseline configuration was longitudinally stable and trimmable at almost all Mach numbers from 0.15 to 10.0--with the exception occurring at low supersonic speeds. Landing speed and subsonic-to-hypersonic longitudinal stability and control appear to be within design guidelines. Lateral-directional instabilities found over the entire speed range, however, create a problem area for this configuration. Longitudinal aerodynamic predictions made utilizing the Aerodynamic Preliminary Analysis System (APAS) were in qualitative, often quantitative agreement with experimental values.

NOMENCLATURE

b	wing span, in.
$\bar{c}$	mean aerodynamic chord, in.
C_A	axial-force coefficient
C_D	drag coefficient
C_l	rolling-moment coefficient
$C_{l\beta}$	$dC_l/d\beta$, per degree
C_m	pitching-moment coefficient
C_N	normal-force coefficient
C_n	yawing-moment coefficient
$C_{N\alpha}$	$dC_N/d\alpha$, per degree
$C_{N\beta}$	$dC_N/d\beta$, per degree
C_Y	side-force coefficient
$C_{Y\beta}$	$dC_Y/d\beta$, per degree
L	fuselage length, in.
L/D or C_L/C_D	lift-to-drag ratio
M	Mach number
R_N	Reynolds number based on L
S_{REF}	wing reference area, $in.^2$
T	temperature, °R
X_{CG}	center of gravity (moment reference center), 67 percent L
α	angle of attack, degrees

---

* Aerospace Engineer, Aerothermodynamics Branch, Research Technology Group, Associate Fellow, AIAA.

§ Aerospace Engineer, Vehicle Analysis Branch, Space and Atmospheric Sciences Program Group, Member, AIAA.

β	angle of sideslip, degrees
δ	control surface deflection angle, degrees (+ for trailing edge down)

Subscripts:

B/F	body flap
e	elevon
max	maximum
o	minimum
t	reservoir condition
trim	longitudinally trimmed condition
v	tip fins
w	model surface; wall surface
∞	free-stream condition

INTRODUCTION

Future space transportation systems proposed for use in the twenty-first century will, by necessity, be less expensive (in both initial and operational costs), provide for reduced turn-around time and operate in a more efficient manner. These requirements point collectively toward a fully reusable, single-stage-to-orbit vehicle (SSV) system lacking in undue operational complexity as being a leading candidate for satisfying this need (e.g., the NASA-Access to Space Study recommendations of Ref. 1). The aerodynamic study of generic, SSV vehicles began within the Langley Aerothermodynamics Branch (formerly the Experimental Hypersonics Branch) in concert with the Advanced Manned Launch System (AMLS) study of Ref. 2. The objectives of this experimental study were to develop an aerodynamically viable, horizontal-landing, single-stage-to-orbit vehicle (SSV), provide an extensive aerodynamic database at subsonic, supersonic, and hypersonic flow conditions and finally to compare engineering code-predicted aerodynamics with the experimental results. The present configuration is an "aerodynamically refined version" of a conceptual lox/hydrogen rocket-powered SSV which resulted from a preliminary computer-aided vehicle design study (Ref. 3). The configuration of Ref. 3, shown in the upper part of Fig. 1, incorporated a "bubble" canopy and an abruptly faired forebody-fuselage interface which produced severe flow separations at approach and landing angles of attack (hence, the nonlinear pitching moment variation--labeled "Original" of Fig. 1). The flow separation problem was solved by removing the canopy, increasing the forebody length, and improving the faring of the fuselage-forebody interface as shown in the "Modified" model photograph (Fig. 1). This produced the significantly more linear pitching-moment curve shown for the configuration with the modified fuselage. Subsequently changes in wing location and planform were incorporated into the present configuration to minimize low speed trim penalties in order to reduce projected landing speeds.

The purpose of this paper is to present aerodynamic characteristics for the winged, circular-body, single-stage-to-orbit spacecraft configuration which evolved experimentally. These results were obtained at Mach numbers of 0.15, 1.6, 2.0, 2.3, 2.96, 3.95, 4.63, 6.0 and 10.0 in air. Tests were conducted in the ViGYAN Research Associates 3 Ft. x 4 Ft. Low-Speed Wind Tunnel, the NASA-Langley Unitary Plan Wind Tunnel, the Langley 20 Inch Mach 6 Tunnel, and the Langley 31 Inch Mach 10 Tunnel at Reynolds numbers (based on model fuselage lengths) from about 0.92×10^6 to 3.42×10^6. Subsonic and supersonic force and moment measurements were obtained at angles of attack from approximately -4° to 20° and fixed sideslip angles of 0° and 5°. Hypersonic measurements were made over an angle-of-attack range from about 0° to 38° at fixed sideslip angles of 0° and -2°. These experimental characteristics are compared with aerodynamics predicted using the Aerodynamic Preliminary Analysis System (APAS) (Ref. 4) as part of the effort to calibrate the engineering codes.

METHOD

Models

The Single Stage Vehicle (SSV) models utilized in the present study are shown schematically in Fig. 2 and in the photographs of Fig. 3. A 28.00 inch long model (Fig. 2(a)) was used in the subsonic investigation while a 10.00 inch long model (Fig. 2(b)) was tested at supersonic and hypersonic Mach numbers. A geometry difference existed in the low-speed model fuselage which had a lower fineness ratio (5.83) than the design fineness ratio of 6.5. This 10 percent lower fineness ratio is not a significant factor for low speed tests. The high-speed model, however, was computer-control machined from aluminum and had a surface tolerance within ± 0.003 inch of construction drawing specifications. The (SSV) configuration consists of a circular cross-section fuselage, a low-mounted wing and vertical tip fins. The fuselage had a drooped forebody (positive camber) and a fineness ratio of 6.5 (5.83 for the low-speed model). The wing planform, which was derived from an earlier space shuttle wing design study (Ref. 5) had leading-and trailing-edge sweep angles of 45° and -10°, respectively; modified NACA 0010 stream wise airfoil sections and 7° dihedral. The tip fins had flat plate sections with rounded leading edges. The exposed wings were fitted with partial span elevons capable of deflections from -20° to +10° in 10° increments. A body flap capable of deflections of -10° (low-speed model only), 0° and +10° was included in the models. Also, the low-speed model wing could be moved aft (0.75 in.) to be representative of a vehicle having dual (hydrogen and hydrocarbon) fueled rocket engines. Additional model physical dimensions can be found in Fig. 2.

Facilities and Test Conditions.

The wind tunnel test conditions are shown in Table I. Three Langley wind tunnels and one privately-owned tunnel (ViGYAN 3 Ft. x 4 Ft. Low-Speed Wind Tunnel) were used to cover a Mach range from 0.15 to 10. The physical and operational characteristics for the supersonic and hypersonic facilities can be found in Refs. 6 and 7, respectively. The ViGYAN tunnel is an atmospheric open-return wind tunnel operating at ambient temperatures and a maximum free-stream dynamic pressure of 40 lb./ft.^{2} at a Mach number of about 0.15. All four tunnels use the pitch-pause technique for obtaining force and moment data. The hypersonic facilities employ model injection systems to shelter the model and strain-gage balance from tunnel starting and stopping loads. Injection also prevents undue heating of the model to reduce thermal conduction effects on the balance and model components. This last provision allowed the utilization of an aluminum SSV model in high speed tests of the present study by limiting run times (the time the model was exposed to the high stagnation temperatures of the hypersonic facilities). The angle-of-attack range of the study extended from about -4° to 20° at subsonic speed, -4° to 24° supersonically and 0° to about 38° at the hypersonic Mach numbers. All tests were run at fixed angles of sideslip of 0° and 5° at subsonic and supersonic speeds and 0° and -2° at Mach 10 (sideslip data were not obtained at M = 6). Reynolds numbers, based on fuselage reference length, for the investigation are shown in Table I.

Instrumentation and Setup.

The aerodynamic forces and moments acting on the models were measured with sting-mounted, six-component strain gage balance arrangements. No base or chamber corrections were applied to the data. Corrections have been applied to the angles of attack and sideslip to account for sting and balance deflections under aerodynamic loading. All pitching-moment coefficient data are presented about the vehicle's most forward center of gravity, anticipated to be at the $X_{C.G.}/L = 0.67$ fuselage station for the baselined hydrogen-fueled configuration. Transition was fixed on the fuselage nose and wing surfaces with appropriately sized and located grit strips for all tests at Mach numbers below 6.0 using the technique outlined in Ref. 8.

Engineering Code Predictions.

The Aerodynamic Preliminary Analysis

System (APAS) was used to predict longitudinal aerodynamic characteristics for the high-speed model at supersonic and hypersonic test Mach numbers. The predictions included estimates of longitudinal control effectiveness. The APAS code (Refs. 4 and 9) is an interactive computer program which allows the user to define a geometry model from configuration drawings and to specify the analysis conditions (e.g., wind tunnel test conditions) and the approach to be used. For example, the present predictions were determined using a combination of tangent-cone, tangent-wedge and Prandlt-Meyer expansion methods to approximate pressure distributions over the model surfaces. Empirical techniques were then used to account for the skin friction and base drag coefficients acting on the model at test Mach numbers and Reynolds numbers. The APAS geometry model was composed of approximately three hundred quadrilateral elements.

RESULTS AND DISCUSSION

The experimental aerodynamic results, including the comparison with APAS predictions are presented herein as follows:

Figure No(s).	Effect(s)
Longitudinal Aerodynamics	
4	Low speed trim.
5	Low speed (hydrogen vs. dual fuel).
6-11	Supersonic trim.
12-13	Hypersonic trim.
14-15	Hypersonic Reynolds number.
16-21	Comparison APAS predictions with super/hypersonic experimental data.
22	Summary aerodynamics (experiment and APAS predictions).
Lateral-Directional Characteristics	
23	Low speed aerodynamics including adding tip fins.
24	Super/hypersonic aerodynamics including Mach number effects.

Longitudinal Aerodynamic Characteristics.

The low speed aerodynamic characteristics for the baseline Single Stage Vehicle are shown in Fig. 4 which also shows the effect of varying longitudinal control deflections for trim. Herein are shown the variations of C_L and C_m with alpha (Fig. 4(a)), L/D and C_D versus alpha (Fig. 4(b)) and alpha and C_m versus C_N (Fig. 4(c)). The pitching-moment coefficient data were taken about a moment reference point corresponding to the most forward center of gravity for the hydrogen fueled baseline vehicle ($X_{C.G.}/L = 0.67$). Design goals for the present SSV concept include landing at approximately 200 knots at an angle of attack of 12°. The data of Fig. 4(a) indicate that the configuration can attain a trimmed landing lift coefficient of about 0.42 at 12° angle of attack. Since this configuration's estimated landing weight-to-wing area ratio is approximately 50 lb./ft.^{2}, this lift capability would imply a landing touchdown at about 205 knots, thereby satisfying the landing speed requirement for the vehicle. The maximum level of untrimmed lift-to-drag ratio is slightly higher than 6.0. The pitching-moment coefficient data of Fig. 4(c) are shown as a function of C_N to enable analysis of the trim capability of the baseline configuration for the most aft center-of-gravity location ($X_{C.G.}/L= 0.693$). The diagonal line labeled: ($X_{C.G.}/L= 0.693$) on the figure indicates a condition of longitudinal trim for this most aft center of gravity location. This figure presentation format is used for other Mach numbers (Figs. 6 to 13) to simplify the experimental data analysis. The low speed pitching-moment coefficient variations of Fig. 4(c) show the baseline configuration to be longitudinally stable and trimmable for both the most forward and aft centers of gravity.

An attempt was made to determine gross low speed aerodynamic effects attributable to moving the wing aftward to simulate a dual (hydrogen and hydrocarbon) fueled, geometrically similar SSV configuration. The most forward center of gravity for such a vehicle was estimated to be located at the vehicle's 69 percent length station. In an attempt to represent this alternate vehicle design the wing was moved aft 0.75 in. (corresponding to a movement of 2.68 percent model length). The resulting aerodynamic characteristics for the two configurations are compared in Fig. 5 for each configuration's most forward center of gravity. As can be observed in the figure, both configurations trim near a landing attitude of 12° for the same elevon and body flap deflections and exhibit only insignificant differences in lift and drag characteristics. Therefore, for similar vehicle volumetric requirements and landing wing loadings, one might expect the "dual fuel" configuration to achieve landing speeds and stable longitudinal stability levels comparable to those for the hydrogen fueled SSV configuration.

Figures 6-11 show the aerodynamic characteristics for the baseline SSV configuration at Mach numbers from 1.6 to 4.63 for a series of elevon and body flap deflection angles. Several trends are observed as Mach numbers increase: $(L/D)_{max}$ and C_{N_α} (the slope of the normal force coefficient curve) experience slight reductions; and longitudinal stability levels are drastically reduced (from a very stable condition at M = 1.6 to instability at the highest supersonic Mach numbers). A condition of neutral stability occurs near a Mach number of 2.96 and, for higher supersonic Mach numbers (Figs. 10 and 11), the pitching moment curves begin to have the character typical of hypersonic winged-body configurations--unstable at low angles with a transition to stable levels at high angles of attack.

Additionally, elevon and body flap effectiveness levels (to produce C_N and C_m) were reduced with increasing Mach number. The most significant longitudinal aerodynamic deficiency noted is the inability of the configuration to achieve longitudinal trim in the low-to-moderate angle-of-attack range at low supersonic Mach numbers (e.g., Figs. 6-9) where a minimum trimmed angle of attack capability of about 10° would be a reasonable requirement. This trim problem could possibly be alleviated by slight increases in the elevon chord (area increase) coupled with negative deflections of the body flap, which could not be accomplished for the high-speed model of this study.

At hypersonic speeds (Figs. 12 and 13) the configuration exhibits stable longitudinal trim in the high angle-of-attack range required for hypersonic reentry. Stable trim conditions exist for both forward and aft center-of-gravity conditions at angles of attack in excess of 34°, also a design requirement. Hypersonic $(L/D)_{max}$ levels of approximately 1.4 to 1.6 are achieved at angles of attack near 20°. Figures 14 and 15 show some hypersonic effects of increasing Reynolds number for the configuration with maximum positive longitudinal control deflections ($\delta_e = \delta_{B/F} = +10°$). This determination is important to show the trend of increasing Reynolds numbers toward flight levels on the pitching moment characteristics for the aft center of gravity. The longitudinal characteristics obtained for increasing Reynolds number from 0.92×10^6 to 3.42×10^6 at a Mach number of 6.0 (Fig. 14) and from 0.92×10^6 to 1.83×10^6 at M = 10.0 indicate slight negative, or favorable pitching moment shifts. These trends would indicate the capability of accommodating further aft centers of gravity. Additional effects noted to accompany the hypersonic Reynolds number increases are moderate reductions in axial force coefficient which are indicative of reductions in skin friction drag coefficient.

Comparisons of predicted supersonic and hypersonic aerodynamic characteristics (APAS) with experimentally obtained values may be found in Figs. 16 - 21. These comparisons are shown for the outer boundaries of the longitudinal control deflection envelope (e.g., $\delta_e = -20°$, $\delta_{B/F} = 0°$ to $\delta_e = \delta_{B/F} = +10°$). The APAS trend at the lowest supersonic Mach number (Fig. 16 for M = 1.6) is to over predict C_{N_α} and under predict longitudinal stability levels ($-C_{m_\alpha}$) and the level of axial

force coefficients. Surprisingly, the longitudinal trim point prediction for the forward center of gravity is accurate. The obvious reason for disagreement in prediction with experiment at low supersonic speeds is the present use of the Hypersonic Arbitrary Body Program in APAS which is inappropriate at low supersonic speeds. As Mach numbers increase to hypersonic speeds improvements are seen in the predicted levels of normal force and pitching-moment coefficients. The trend at hypersonic Mach numbers (Figs. 20 and 21) is to under predict axial force and therefore to over predict $(L/D)_{max}$. Predictions of longitudinal trim capability appear to match the experimental data.

Fig. 22 shows summary longitudinal aerodynamic characteristics as a function of Mach number for the experimental study and includes predicted data at supersonic and hypersonic Mach numbers. The experimental values of C_{N_α} and minimum drag coefficient (C_{D_0}) (Fig. 22(a)) at low supersonic speeds are larger than the subsonic levels. As the Mach numbers increase to 10.0, a gradual decline in the levels is shown. The corresponding APAS predicted values are in reasonable agreement with C_{D_0} but the tendency is to over predict C_{N_α} particularly at low supersonic Mach numbers. Experimental supersonic and hypersonic $(L/D)_{max}$ levels (Fig. 22(b)) are substantially lower than the subsonic value of about 6.4 (e.g., 2.2 at M = 1.6 and 1.5 at M = 10). Since these untrimmed $(L/D)_{max}$ levels are higher than similarly obtained values for the space shuttle orbiter (e.g., supporting studies of Ref. 10) the present $(L/D)_{max}$ levels appear to be adequate for reentry, descent, approach, and landing flight for this class vehicle. The lower part of Fig. 22(b) shows the trimmed angle of attack capability for the baseline SSV configuration over the Mach range investigated. The constant band on the figure, which extends from transonic to high supersonic Mach numbers, represents an estimate of the minimum trim angle required ($\alpha = 10°$) during transition flight following reentry and preceding the subsonic glide to landing. The experimental results, as mentioned previously, indicate a trim deficiency at low supersonic Mach numbers and the APAS predictions are in qualitative agreement.

Lateral-Directional Characteristics.

Subsonic lateral-directional aerodynamic characteristics for the configuration are shown in Fig. 23 as are the effects of adding the tip fins to complete the baseline SSV configuration. The configuration without tip fins is directionally unstable over the entire angle-of-attack range. Adding the fins, although producing stabilizing increments, falls short of providing a directionally stable configuration. The tip fin addition also provides favorable lateral stability increments ($-C_{l_\beta}$) which is enough to provide at least neutral lateral stability at landing attitude ($\alpha = 12°$).

The supersonic and hypersonic lateral-directional aerodynamic characteristics (Fig. 24) show the baseline configuration to be directionally unstable at all Mach over the entire angle-of-attack range. Positive effective dihedral is attained only at high angles of attack supersonically. At M = 10.0, the configuration appears to be laterally stable over the anticipated flight angle-of-attack range. The directional instabilities present over the entire Mach number range coupled with marginally stable to unstable lateral characteristics produce severe aerodynamic control problems for the configuration if extensive reliance upon reaction control is to be avoided. The addition to the configuration of a fuselage-mounted vertical tail would tend to alleviate the subsonic lateral-directional stability and control deficiency.

CONCLUDING REMARKS

Experimental longitudinal and lateral-directional aerodynamic characteristics were obtained for a generic hydrogen fueled single-stage-to-orbit concept herein referred to as the SSV configuration. Tests were conducted at low subsonic speeds, supersonic speeds and hypersonic Mach numbers of 6.0 and 10.0. The baseline SSV configuration was longitudinally stable and trimmable at nearly all study Mach numbers--the exception being supersonic Mach numbers from about 1.6 to

2.96 where the control effectiveness was insufficient to trim the vehicle at an angle of attack of 10°. This deficiency could probably be overcome by slightly increasing the elevon size and utilizing a negatively deflected body flap. The configuration's low speed aerodynamic characteristics indicate that it meets the design landing speed requirement for a touchdown speed of approximately 200 knots at an angle of attack of 12°. Untrimmed $(L/D)_{max}$ levels found over the flight Mach number range are indicative of satisfying flight requirements for this class vehicle. In general, the longitudinal aerodynamic predictions of the Aerodynamic Preliminary Analysis System (APAS) were in qualitative, and often, quantitative agreement with measurement, with the accuracy improving with increasing Mach number. The experimentally obtained lateral-directional aerodynamic characteristics indicate the configuration is directionally unstable over the entire Mach range. This instability coupled with marginally stable-to-unstable lateral characteristics indicates a need to modify lateral-directional aerodynamic controls to avoid extensive reliance on the reaction control system.

REFERENCES

1. "Access to Space Study-Summary Report, Office of Space Systems Development," NASA Headquarters, January 1994.

2. Freeman, D. C., Jr.; Wilhite, A. W.; and Talay, T. A.: "Advanced Manned Launch System Study Status," IAF Paper 91-193, 1991.

3. Stanley, D. O.; Engelund, W. C.; Lepsch, R. A.; McMillin, M.; Wurster, K. E.; Powell, R. W. and Guinta, A. A.: "Rocket-Powered Single-Stage Vehicle Configuration Selection and Design," AIAA Paper 93-1053, 1993.

4. Bonner, E.; Clever, W. and Dunn, K: "Aerodynamic Preliminary Analysis System II, Part I-Theory," 1989.

5. Phillips, W. P.; Decker, J. P.; Rau, T. R. and Glatt, C. R.: "Computer-aided Space Shuttle Orbiter Wing Design Study," NASA TN D-7478, May 1974.

6. Jackson, C. M.., Jr.; Corlett, W. A. and Monta, W. J.: "Description and Calibration of the Unitary Plan Wind Tunnel," NASA TP 1905, November 1981.

7. Miller, C. G., III: "Langley Hypersonic Aerodynamic/ Aerothermodynamic Testing Capabilities-Present and Future," AIAA Paper 90-1376, 1990.

8. Braslow, A. L. and Knox, E. C.: "Simplified Method for Determination of Critical Height of Distributed Roughness Particles for Boundary-Layer Transition at Mach Numbers from 0 to 5," NACA TN 4363, 1958.

9. Cruz, C. I. and Wilhite, A. W.: "Prediction of High Speed Aerodynamic Characteristics Using the Aerodynamic Preliminary Analysis System (APAS)," IA Paper 89-2123, 1989.

10. Scallion, W. I. and Phillips, W. P.: "Space Shuttle Orbiter Trimmed Center-of-Gravity Extension Study," NASA TP 2284, 1985.

TABLE I-WIND TUNNEL TEST CONDITIONS

FACILITY	MACH NO.	$R_N \times 10^{-6}$	T_t,°R	T_w/T_t
ViGYAN	0.15	2.8	520	----
UPWT	1.6 - 4.63	1.67	585	----
20-IN.M6	6	0.92 - 3.42	805	0.6
31-IN.M10	10	0.92 - 1.83	1840	0.3

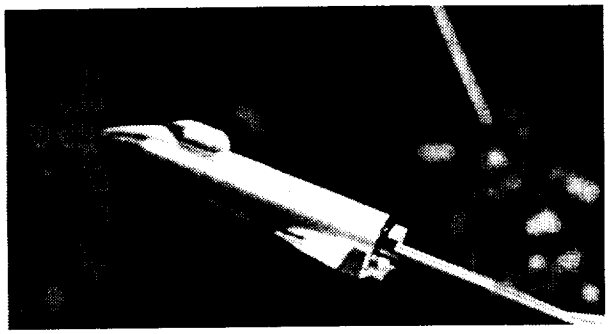

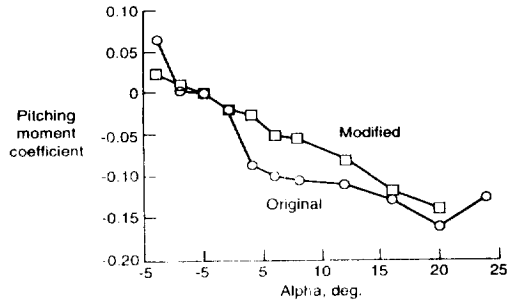

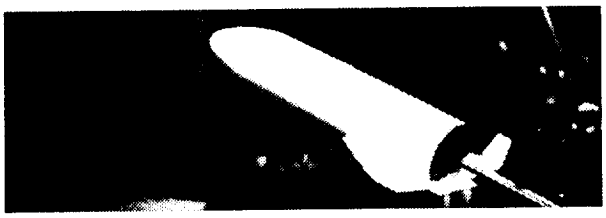

Fig. 1 Effect of removing the "bubble" canopy and refairing the forebody-fuselage interface of the Ref. 3 SSV configuration.

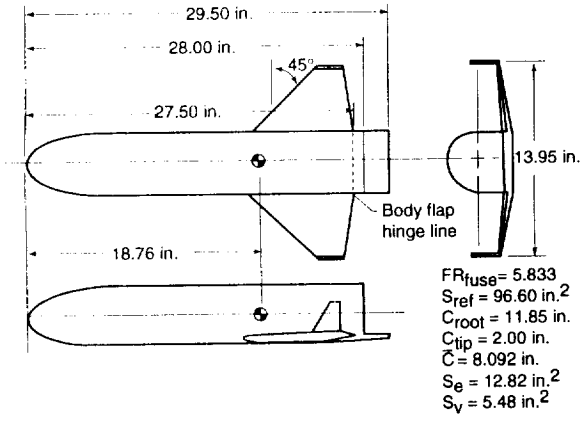

(a) 28.00 inch low-speed model

Fig. 2 Schematics of wind tunnel models.

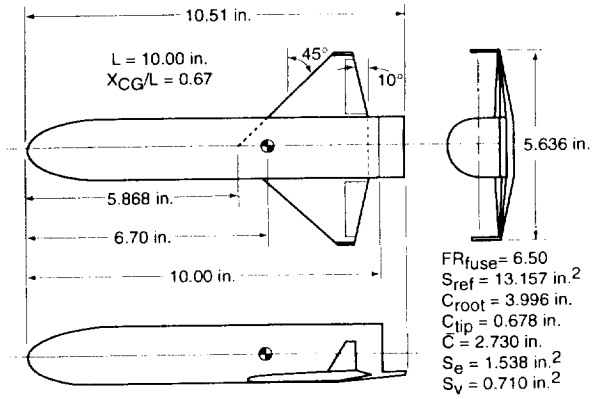

(a) 10.00 inch high-speed model

Fig. 2 Concluded

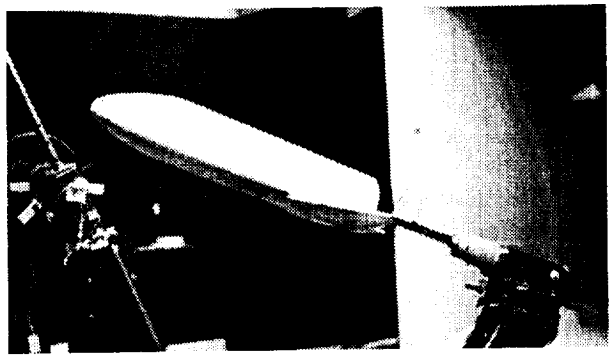

(a) Low-speed (28.00 in. long) model in the ViGYAN 3 FT. X 4 FT. Wind Tunnel.

Fig. 3 Single Stage Vehicle wind tunnel models.

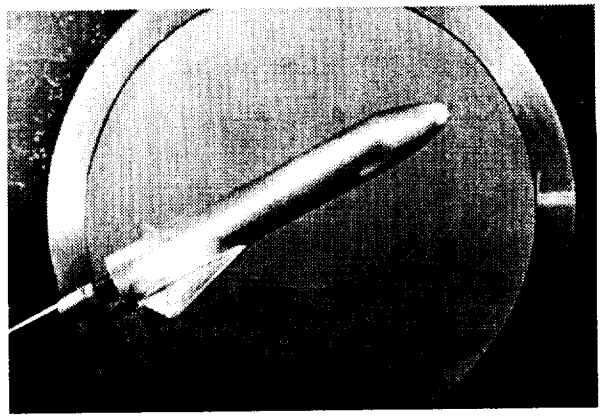

(b) High-speed (10.00 in. long) model in the Langley 20 Inch Mach 6 Tunnel.

Fig. 3 Concluded.

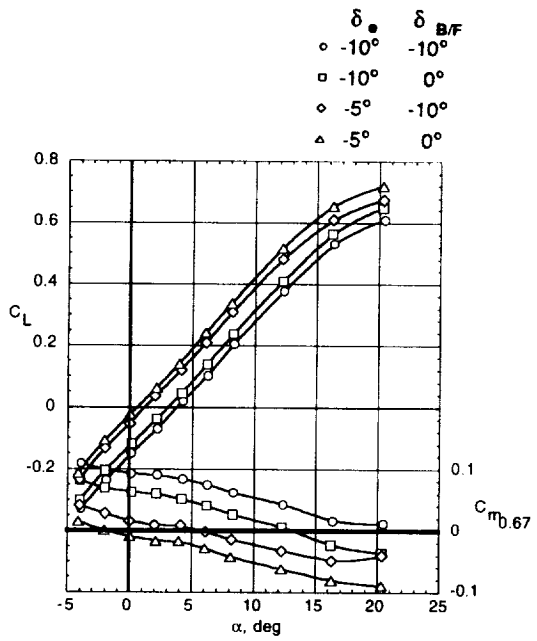

(a) C_L, C_m versus alpha.

Fig. 4 Subsonic longitudinal aerodynamic characteristics for the Single Stage Vehicle configuration.

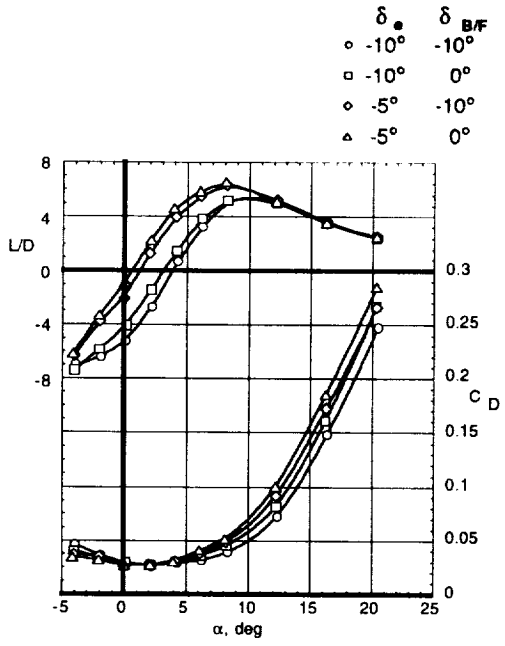

(b) L/D, C_A versus alpha.

Fig. 4 Continued.

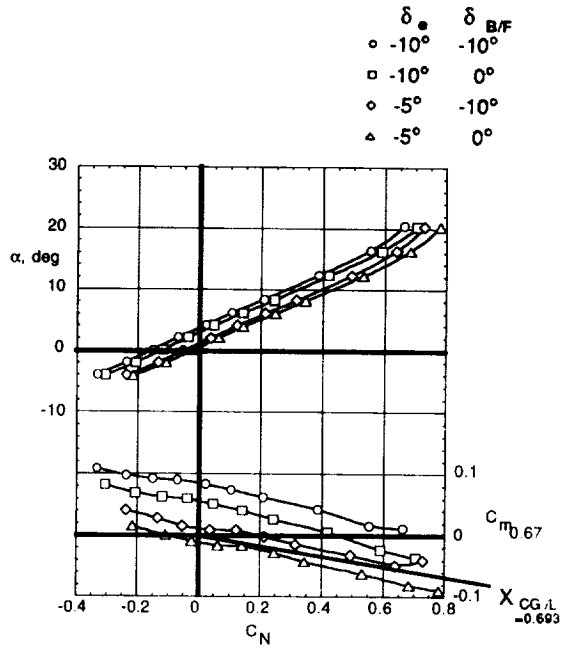

(c) Alpha, C_m versus C_N.

Fig. 4 Concluded.

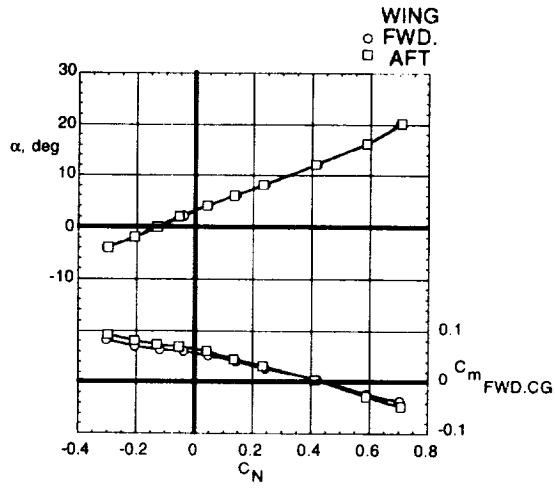

(a) Alpha, C_m versus C_N.

Fig. 5 Effect of moving the wing aft 0.75 in. (simulating a change in rocket fuel--from H_2 to a dual fuel) on the subsonic longitudinal aerodynamic characteristics. δ_e = -10°; $\delta_{B/F}$ = -10°.

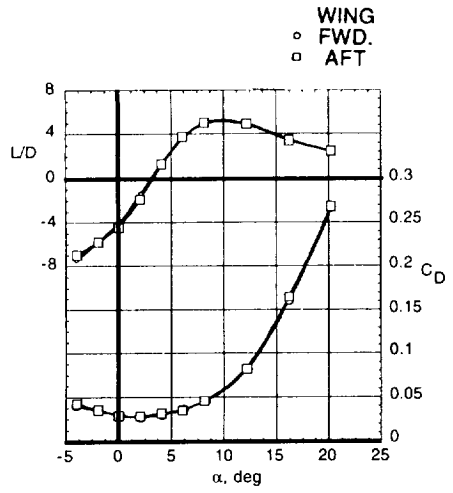

(b) L/D, C_A versus alpha.

Fig. 5 Concluded.

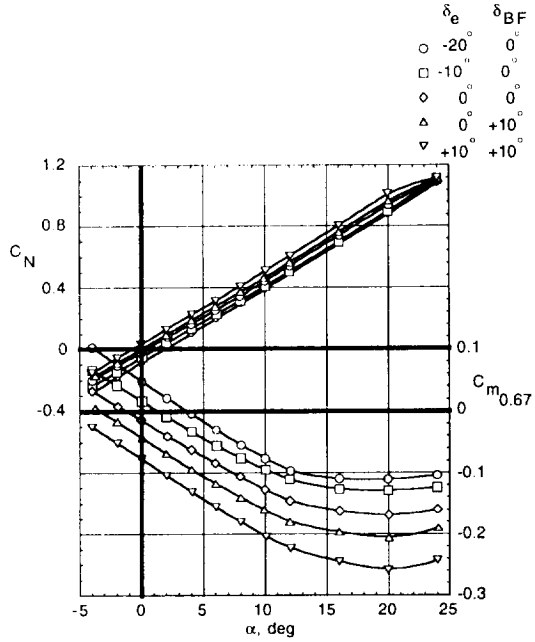

(a) C_N, C_m versus alpha.

Fig. 6 Effect of deflecting the longitudinal controls (elevons and body flap) on the longitudinal aerodynamic characteristics for the SSV configuration at $M = 1.6$ and $R_N = 1.67 \times 10^6$.

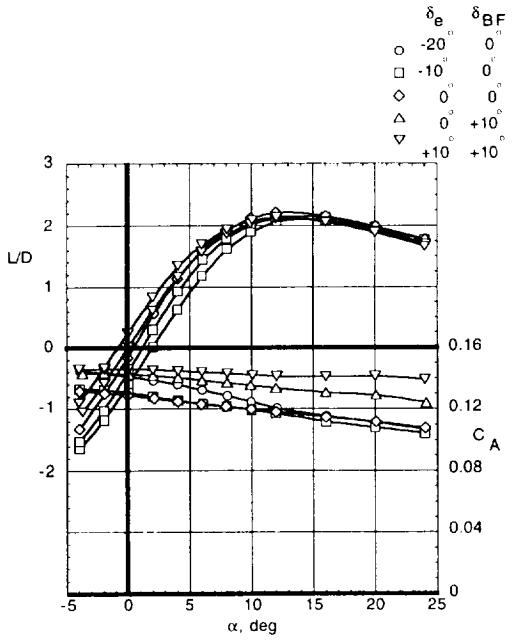

(b) L/D, C_A versus alpha.

Fig. 6 Continued.

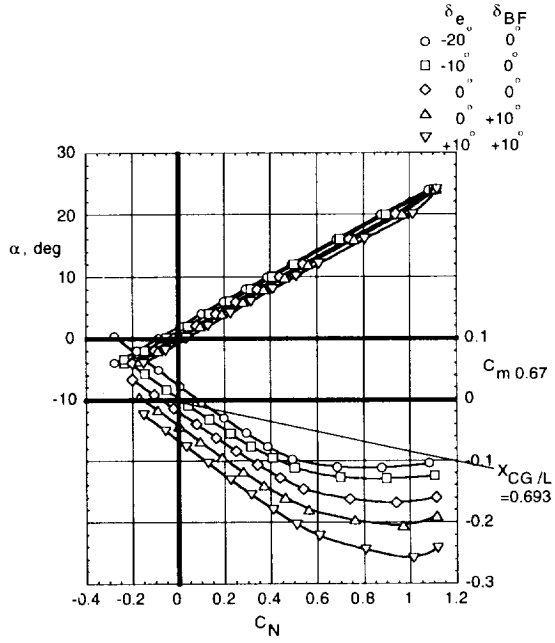

(c) Alpha, C_m versus C_N.

Fig. 6 Concluded.

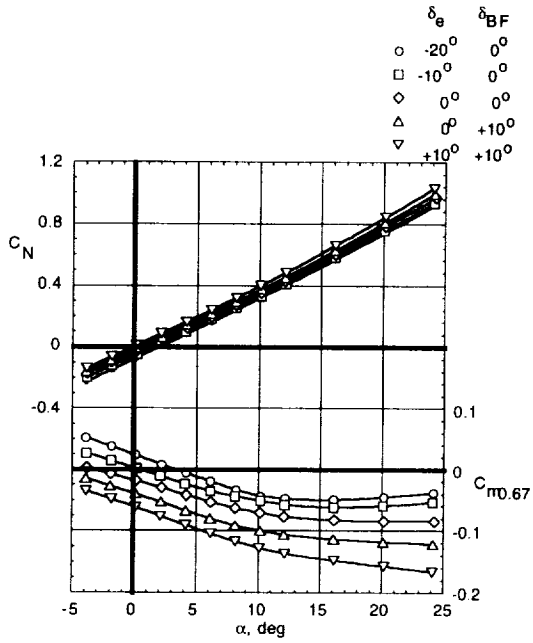

(a) C_N, C_m versus alpha.

Fig. 7 Effect of deflecting the longitudinal controls (elevons and body flap) on the longitudinal aerodynamic characteristics for the SSV configuration at $M = 2.0$ and $R_N = 1.67 \times 10^6$.

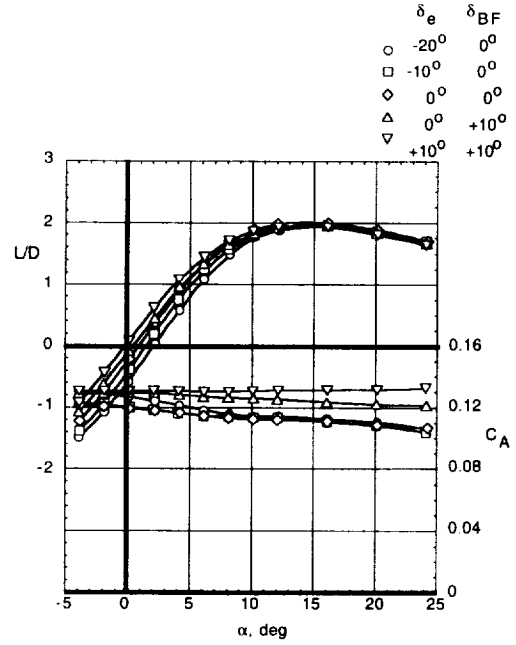

(b) L/D, C_A versus alpha.

Fig. 7 Continued.

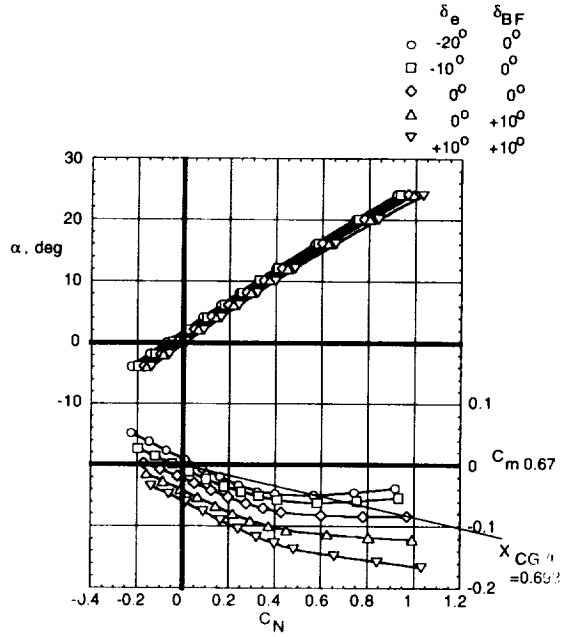

(c) Alpha, C_m versus C_N.

Fig. 7 Concluded.

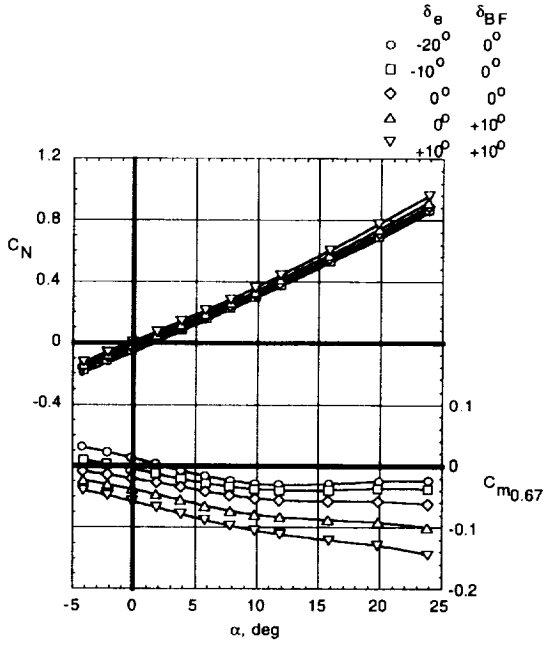

(a) C_N, C_m versus alpha.

Fig. 8 Effect of deflecting the longitudinal controls (elevons and body flap) on the longitudinal aerodynamic characteristics for the SSV configuration at $M = 2.3$ and $R_N = 1.67 \times 10^6$.

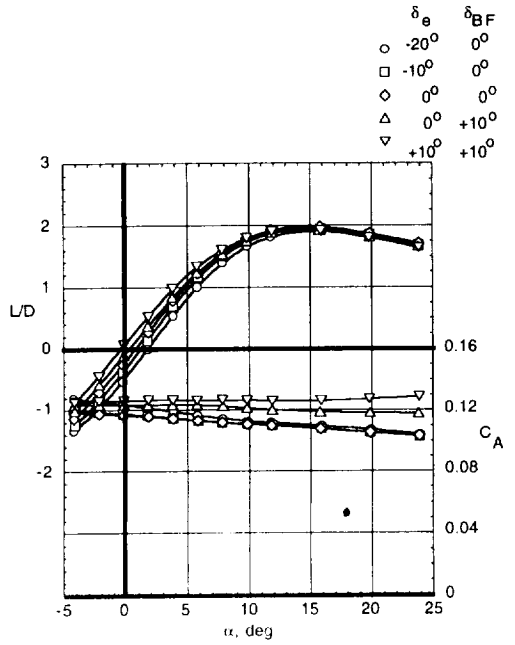

(b) L/D, C_A versus alpha.

Fig. 8 Continued.

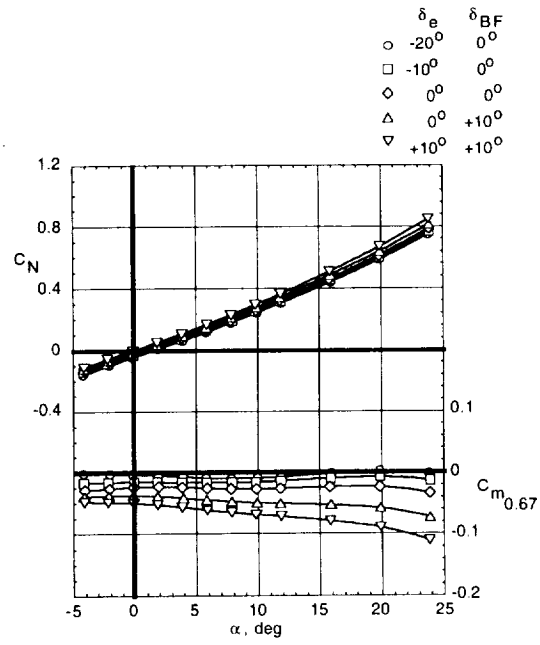

(a) C_N, C_m versus alpha.

Fig. 9 Effect of deflecting the longitudinal controls (elevons and body flap) on the longitudinal aerodynamic characteristics for the SSV configuration at $M = 2.96$ and $R_N = 1.67 \times 10^6$.

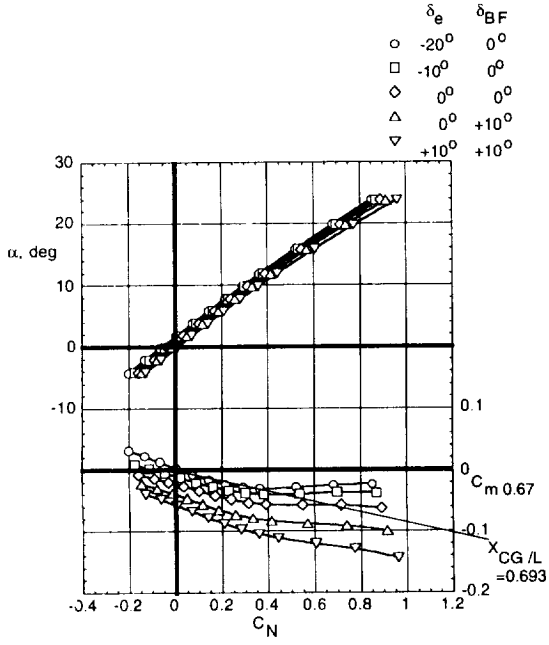

(c) Alpha, C_m versus C_N.

Fig. 8 Concluded.

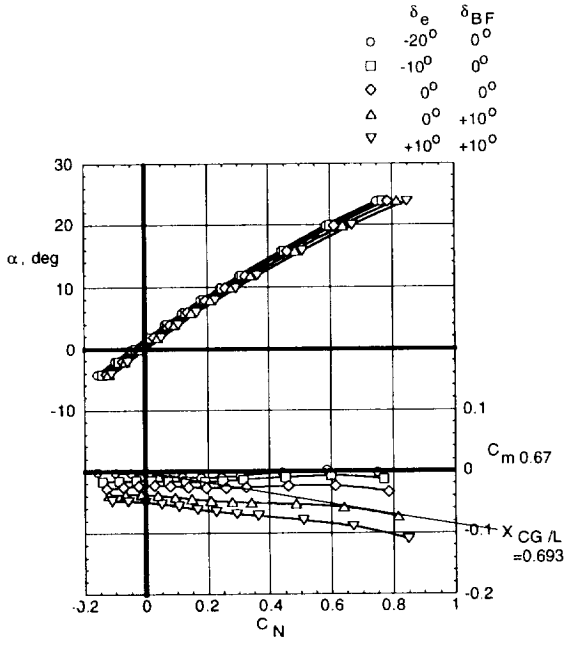

(b) L/D, C_A versus alpha.

Fig. 9 Continued.

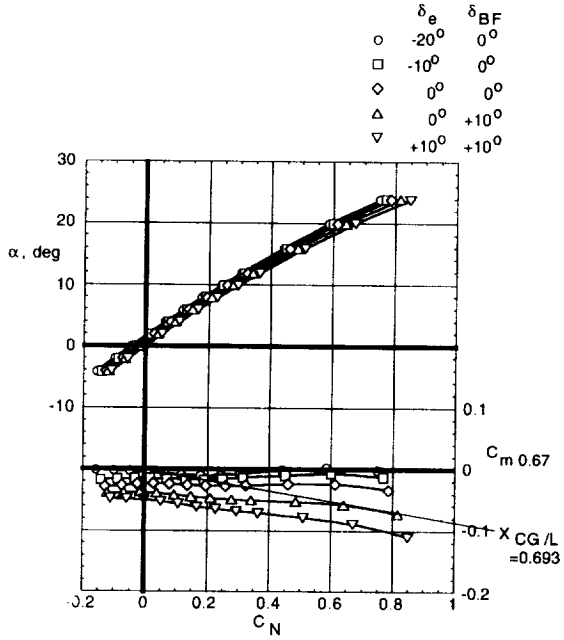

(c) Alpha, C_m versus C_N.

Fig. 9 Concluded.

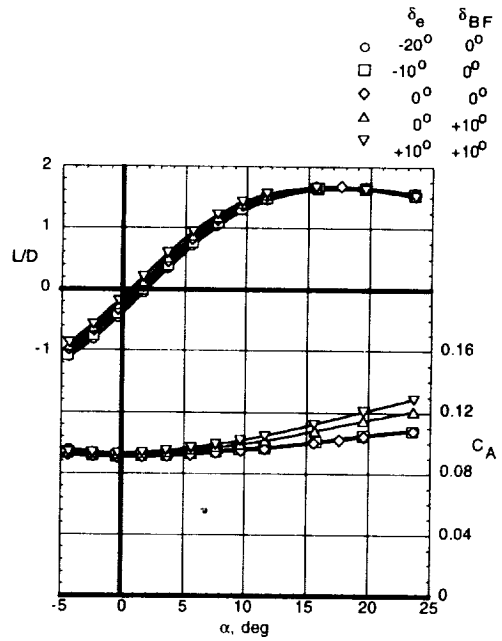

(b) L/D, C_A versus alpha.

Fig. 10 Continued.

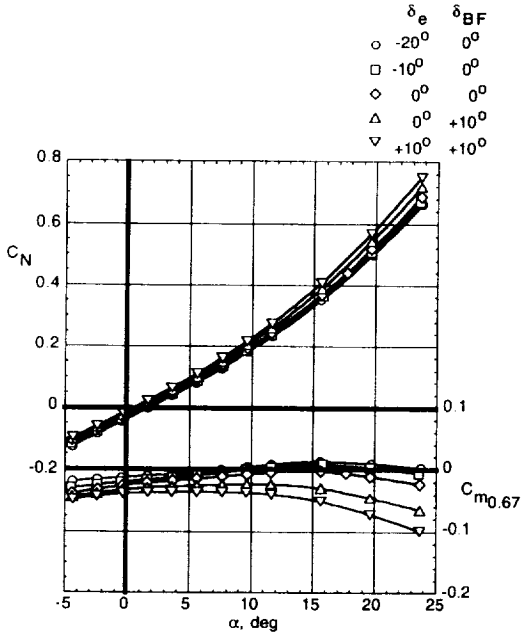

(a) C_N, C_m versus alpha.

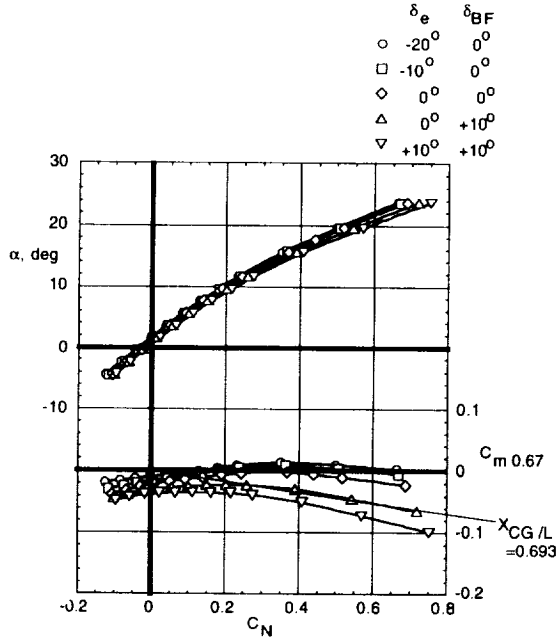

(c) Alpha, C_m versus C_N.

Fig. 10 Effect of deflecting the longitudinal controls (elevons and body flap) on the longitudinal aerodynamic characteristics for the SSV configuration at $M = 3.95$ and $R_N = 1.67 \times 10^6$.

Fig. 10 Concluded.

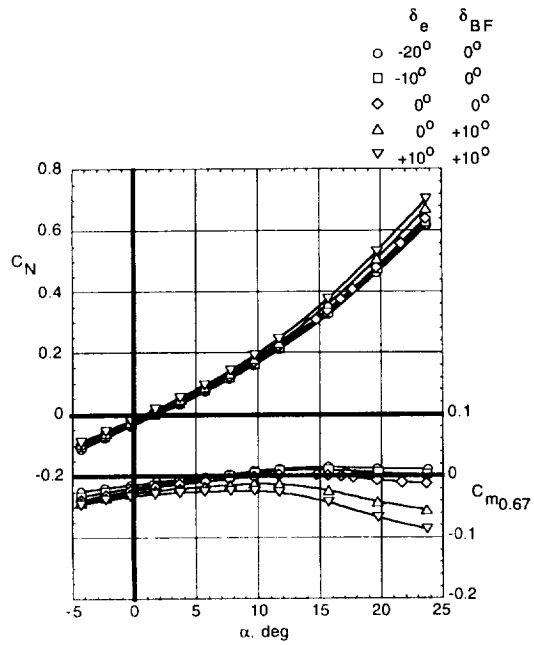

(a) C_N, C_m versus alpha.

Fig. 11 Effect of deflecting the longitudinal controls (elevons and body flap) on the longitudinal aerodynamic characteristics for the SSV configuration at $M = 4.63$ and $R_N = 1.67 \times 10^6$.

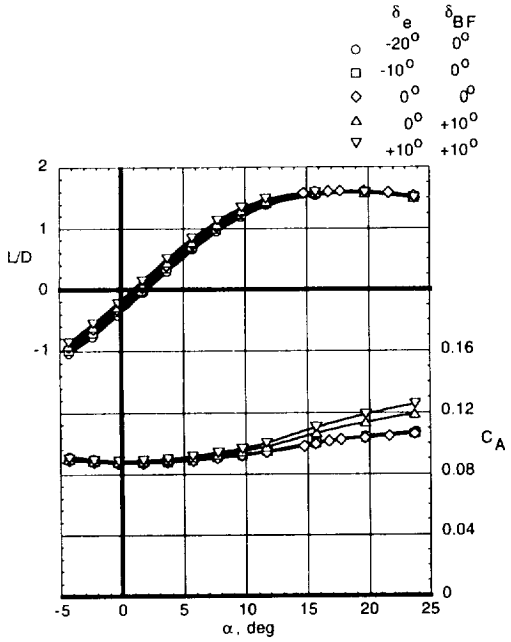

(b) L/D, C_A versus alpha.

Fig. 11 Continued.

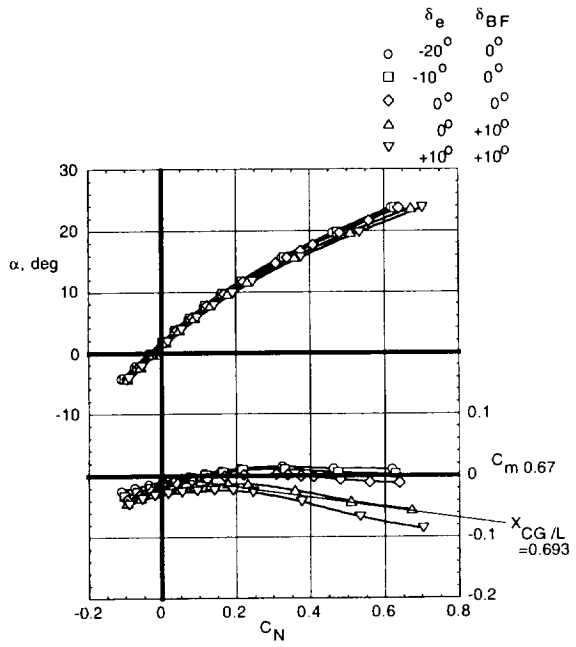

(c) Alpha, C_m versus C_N.

Fig. 11 Concluded.

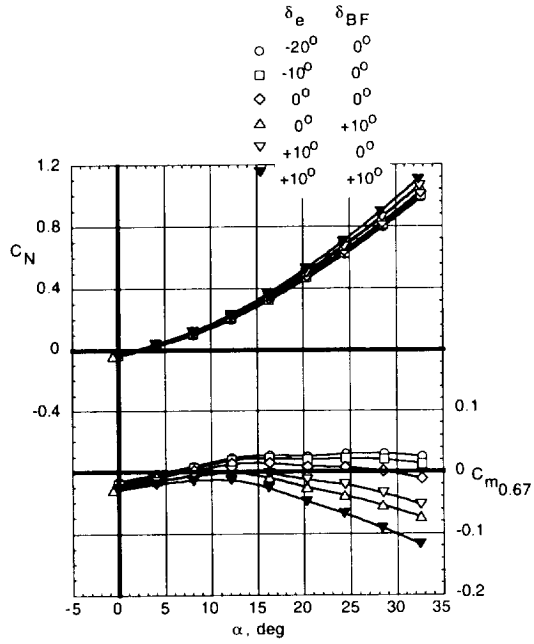

(a) C_N, C_m versus alpha.

Fig. 12 Effect of deflecting the longitudinal controls (elevons and body flap) on the longitudinal aerodynamic characteristics for the SSV configuration at $M = 6.0$ and $R_N = 2.33 \times 10^6$.

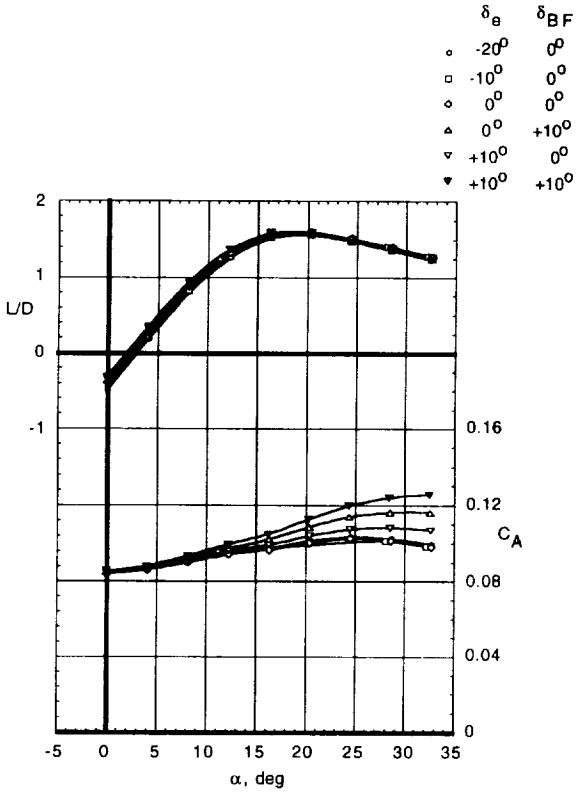

(b) L/D, C_A versus alpha.

Fig. 12 Continued.

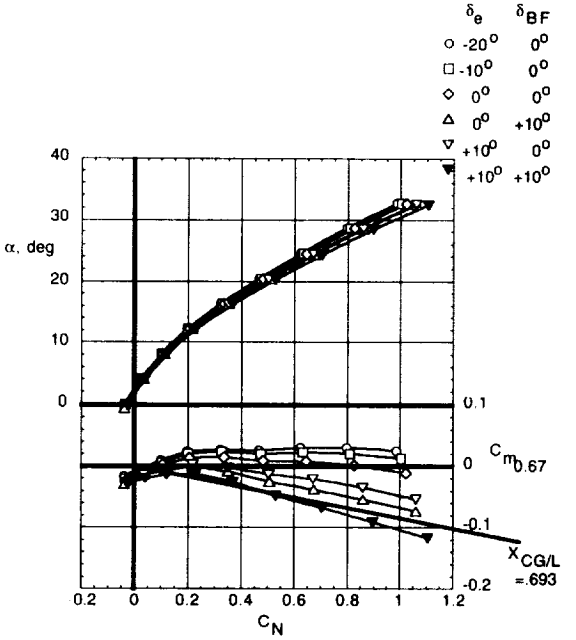

(c) Alpha, C_m versus C_N.

Fig. 12 Concluded.

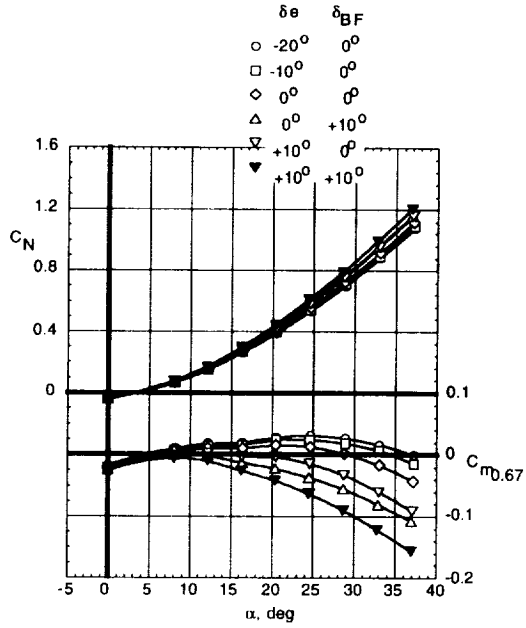

(a) C_N, C_m versus alpha.

Fig. 13 Effect of deflecting the longitudinal controls (elevons and body flap) on the longitudinal aerodynamic characteristics for the SSV configuration at $M = 10.0$ and $R_N = 1.83 \times 10^6$.

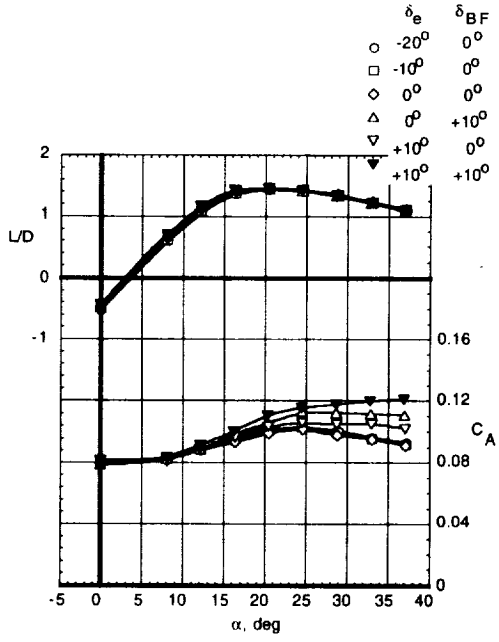

(b) L/D, C_A versus alpha.

Fig. 13 Continued.

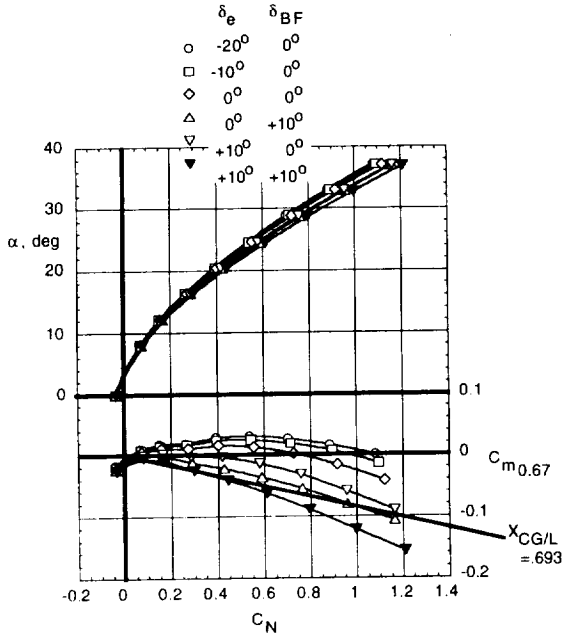

(c) Alpha, C_m versus C_N.

Fig. 13 Concluded.

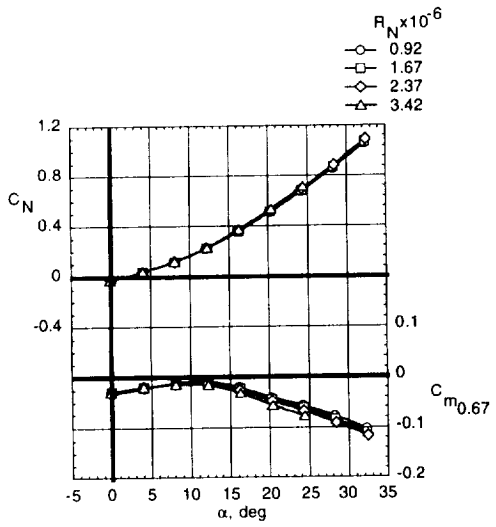

(a) C_N, C_m versus alpha.

Fig. 14 Effect of increasing Reynolds number on the longitudinal aerodynamic characteristics for the SSV configuration at M = 6.0. δ_e = +10°; $\delta_{B/F}$ = +10°.

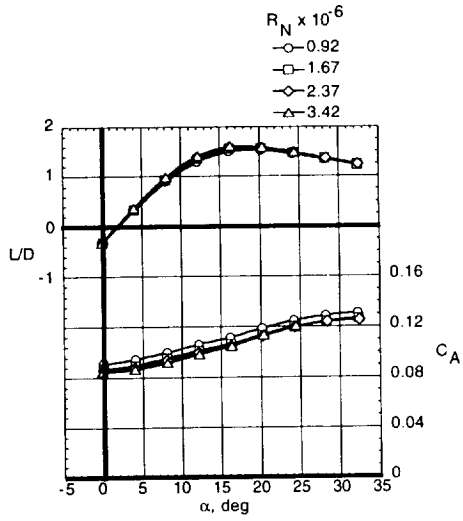

(b) L/D, C_A versus alpha.

Fig. 14 Concluded.

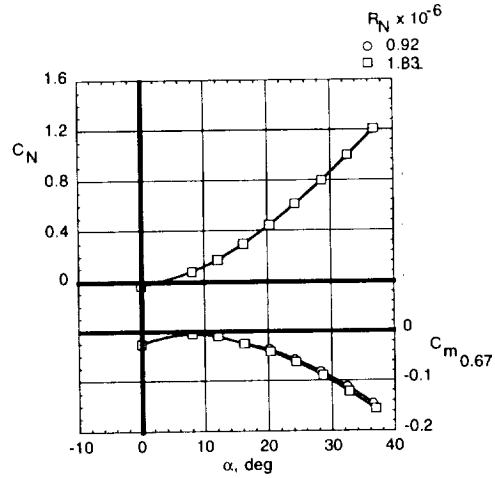

(a) C_N, C_m versus alpha.

Fig. 15 Effect of increasing Reynolds number on the longitudinal aerodynamic characteristics for the SSV configuration at M = 10.0. δ_e = +10°; $\delta_{B/F}$ = +10°.

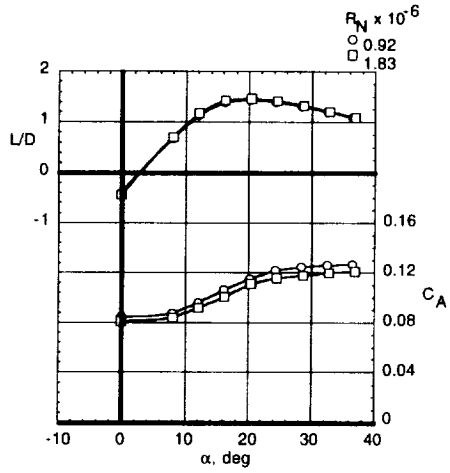

(b) L/D, C_A versus alpha.

Fig. 15 Concluded.

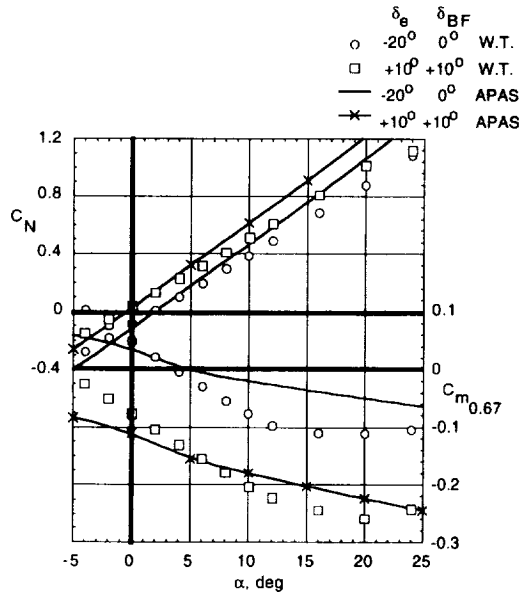

(a) C_N, C_m versus alpha.

Fig. 16 Comparison of predicted longitudinal aerodynamics (APAS) with experimentally obtained values for the SSV configuration having extreme elevon and body flap deflections at M = 1.6 and $R_N = 1.67 \times 10^6$.

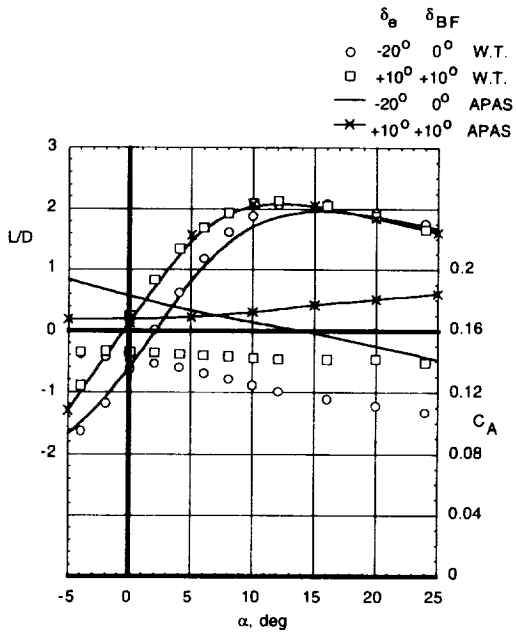

(b) L/D, C_A versus alpha.

Fig. 16 Concluded.

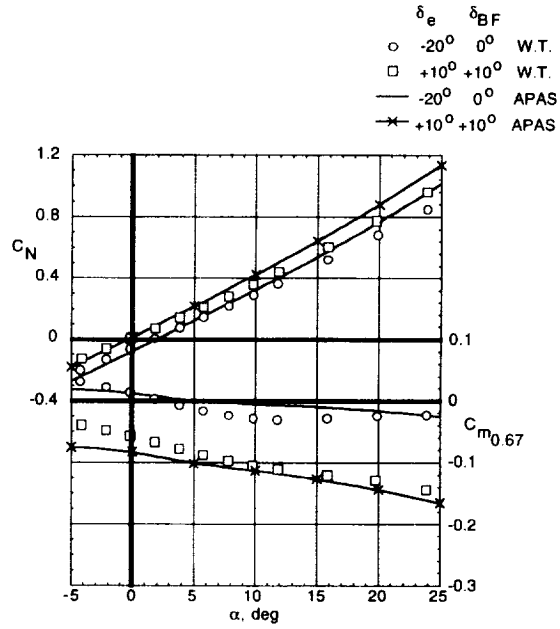

(a) C_N, C_m versus alpha.

Fig. 17 Comparison of predicted longitudinal aerodynamics (APAS) with experimentally obtained values for the SSV configuration having extreme elevon and body flap deflections at M = 2.3 and $R_N = 1.67 \times 10^6$.

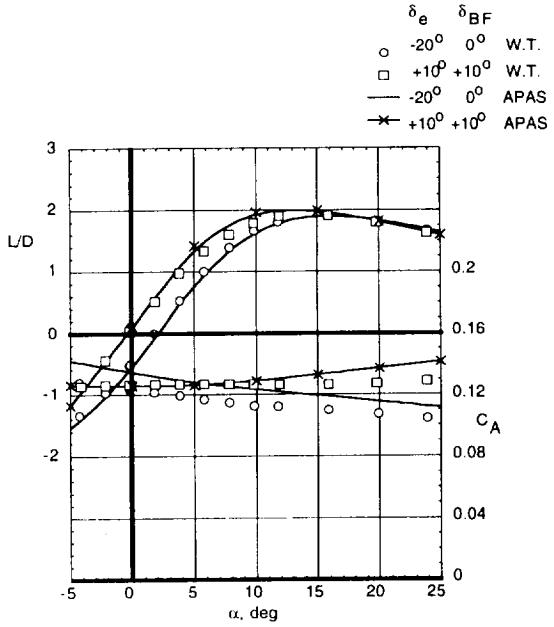

(b) L/D, C_A versus alpha.

Fig. 17 Concluded.

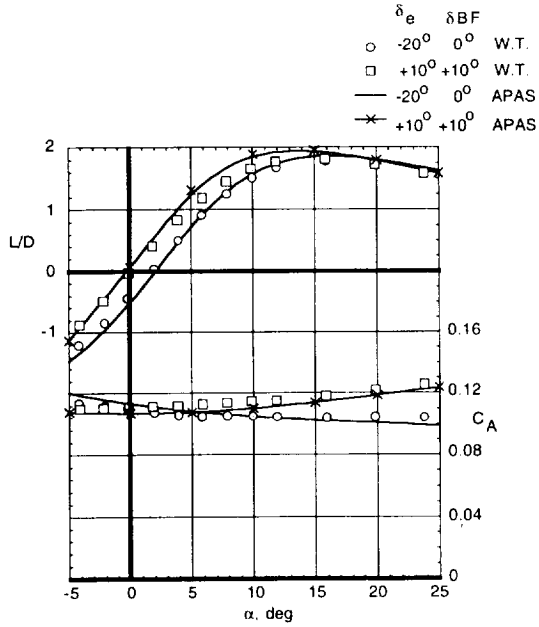

(b) L/D, C_A versus alpha.

Fig. 18 Concluded.

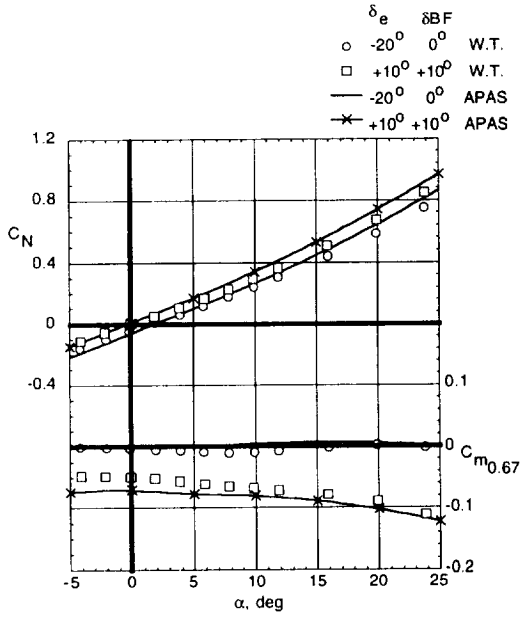

(a) C_N, C_m versus alpha.

Fig. 18 Comparison of predicted longitudinal aerodynamics (APAS) with experimentally obtained values for the SSV configuration having extreme elevon and body flap deflections at
M = 2.96 and R_N = 1.67 x 10^6.

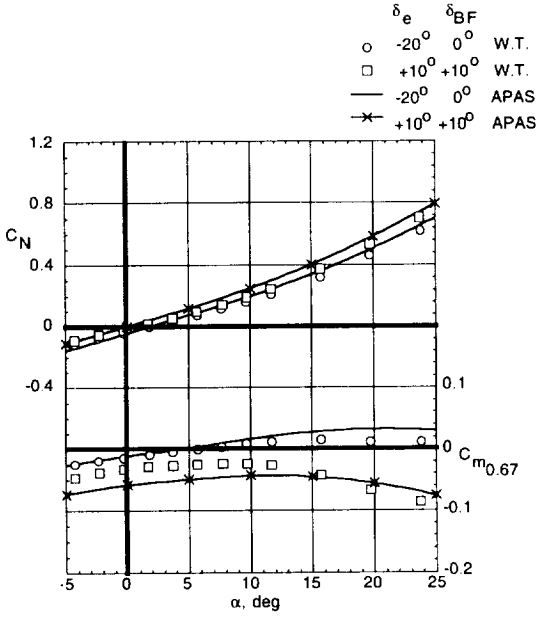

(a) C_N, C_m versus alpha.

Fig. 19 Comparison of predicted longitudinal aerodynamics (APAS) with experimentally obtained values for the SSV configuration having extreme elevon and body flap deflections at
M = 4.63 and R_N = 1.67 x 10^6.

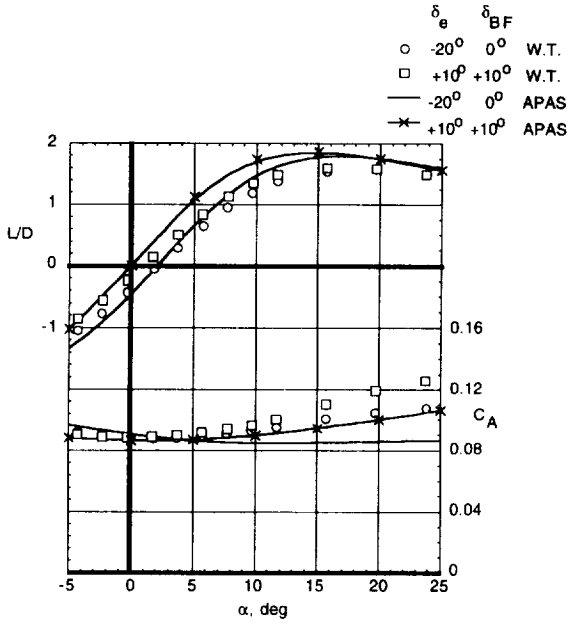

(b) L/D, C_A versus alpha.

Fig. 19 Concluded.

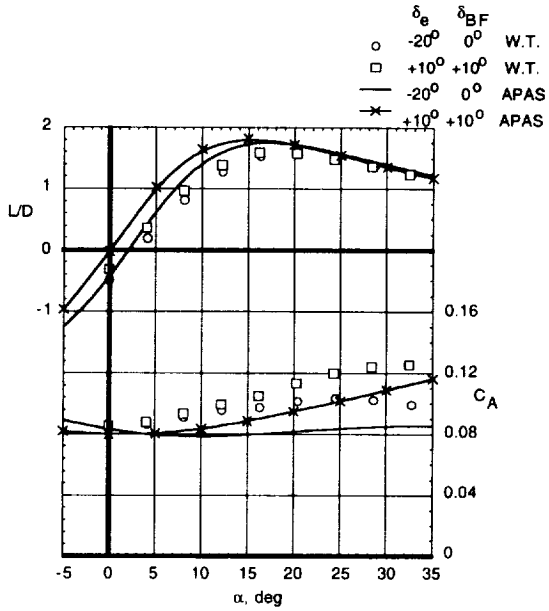

(b) L/D, C_A versus alpha.

Fig. 20 Concluded.

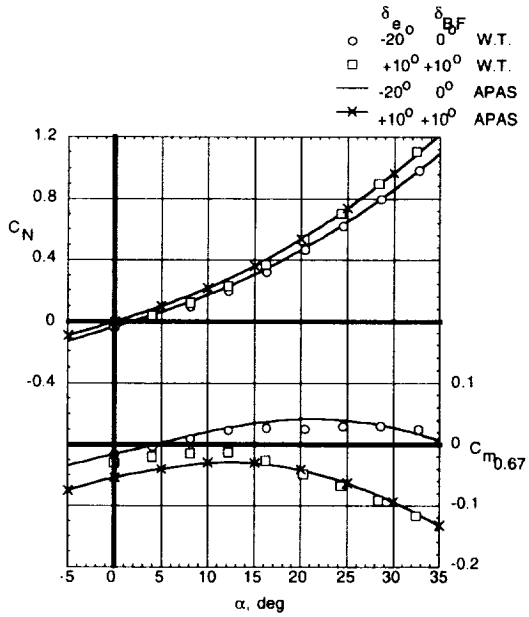

(a) C_N, C_m versus alpha.

Fig. 20 Comparison of predicted longitudinal aerodynamics (APAS) with experimentally obtained values for the SSV configuration having extreme elevon and body flap deflections at
M = 6.0 and R_N = 2.33 x 10^6.

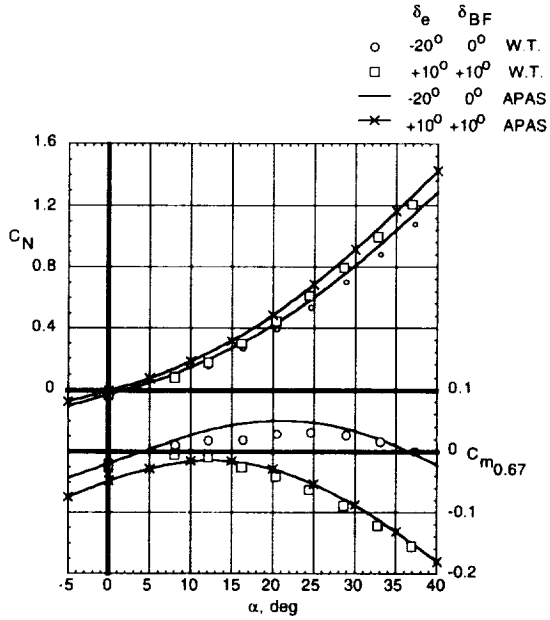

(a) C_N, C_m versus alpha.

Fig. 21 Comparison of predicted longitudinal aerodynamics (APAS) with experimentally obtained values for the SSV configuration having extreme elevon and body flap deflections at
M = 10.0 and R_N = 1.83 x 10^6.

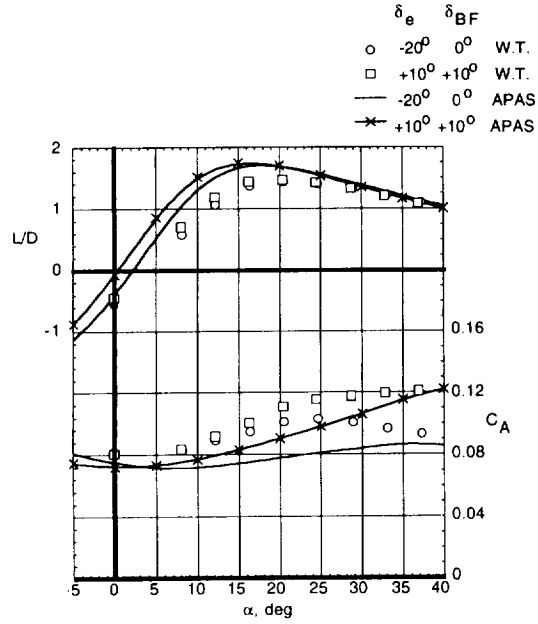

(b) L/D, C_A versus alpha.

Fig. 21 Concluded.

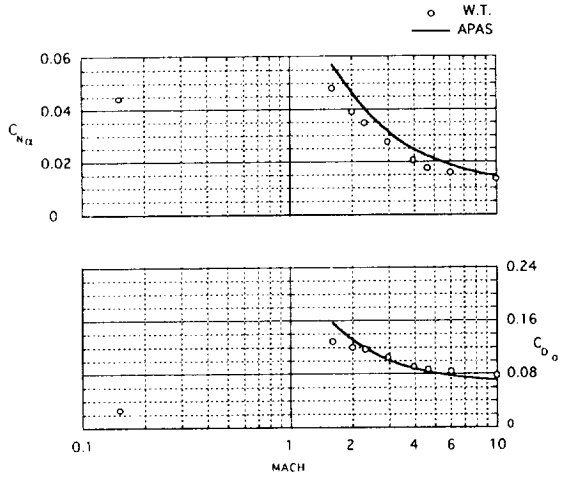

(a) C_{N_α}, C_{D_0} versus Mach number.

Fig. 22 Summary of longitudinal aerodynamic parameters for the Single Stage Vehicle. $1.67 \times 10^6 \leq R_N \leq 2.8 \times 10^6$.

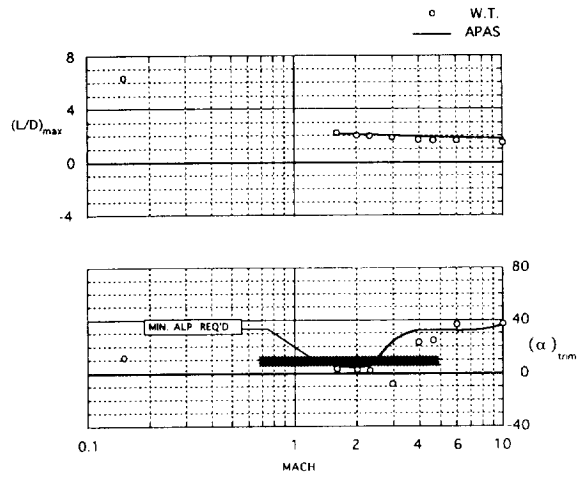

(b) $(L/D)_{max}$, $(\alpha)_{trim}$ versus Mach number.

Fig. 22 Concluded.

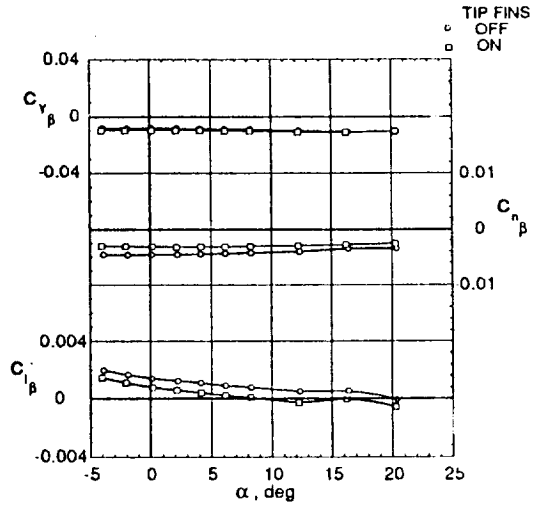

Fig. 23 Effect of adding the tip fins on the subsonic lateral-directional aerodynamic characteristics for the Single Stage Vehicle. M = 0.15 and $R_N = 2.8 \times 10^6$.

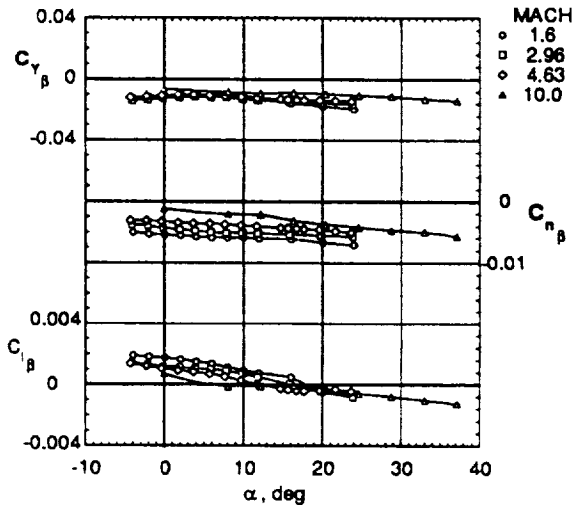

Fig. 24 Lateral-directional aerodynamic characteristics for the SSV configuration at various supersonic and hypersonic Mach numbers for undeflected longitudinal controls ($\delta_e = 0^o$; $\delta_{B/F} = 0^o$). $1.67 \times 10^6 \leq R_N \leq 1.83 \times 10^6$.